Journal of Catalysis 285 (2012) 6–9

Contents lists available at SciVerse ScienceDirect

Journal of Catalysis

journal homepage: www.elsevier.com/locate/jcat

Hydrogen spillover monitored by resonant photoemission spectroscopy

Yaroslava Lykhach [a,*], Thorsten Staudt [a], Mykhailo Vorokhta [b], Tomáš Skála [c], Viktor Johánek [b], Kevin C. Prince [c], Vladimír Matolín [b], Jörg Libuda [a,d]

[a] Lehrstuhl für Physikalische Chemie II, Department Chemie und Pharmazie, Friedrich-Alexander-Universität Erlangen-Nürnberg, Egerlandstr. 3, 91058 Erlangen, Germany
[b] Charles University, Faculty of Mathematics and Physics, Department of Surface and Plasma Science, V Holešovičkách 2, 18000 Prague 8, Czech Republic
[c] Sincrotrone Trieste SCpA, Strada Statale 14, km 163.5, 34149 Basovizza-Trieste, Italy
[d] Erlangen Catalysis Resource Center and Interdisciplinary Center Interface Controlled Processes, Friedrich-Alexander-Universität Erlangen-Nürnberg, Egerlandstr. 3, 91058 Erlangen, Germany

ARTICLE INFO

Article history:
Received 24 May 2011
Revised 26 August 2011
Accepted 1 September 2011
Available online 4 October 2011

Keywords:
Ceria
Platinum
Hydrogen
Hydrogen spillover
Model catalyst
Heterogeneous catalysis
Resonant photoemission spectroscopy

ABSTRACT

We have employed resonant photoemission spectroscopy to investigate the phenomenon of hydrogen spillover on well-defined model Pt/ceria catalysts. On Pt/CeO_2(111)/Cu(111), hydrogen spillover and reverse spillover give rise to reversible changes of the oxidation state of the surface cerium ions. These changes are monitored with highest sensitivity via resonant enhancement of Ce^{3+}- and Ce^{4+}-related features in the valence band photoemission spectra. The temperature regions are precisely determined in which specific processes such hydrogen spillover, Ce^{3+} transport, and reverse spillover are activated.

1. Introduction

In modern catalysis research, the phenomenon of spillover has been a subject of intense investigations [1–12]. Conceptually, the term describes the transfer of an activated species via surface diffusion from an active particle to the support (spillover) or vice versa (reverse spillover). Spillover processes, in particular, involving hydrogen, have suggested to be implicated in the mechanisms of many catalytic processes, including, e.g., methanol synthesis, the water gas shift reaction, Fischer–Tropsch synthesis, or hydrogenation reactions [10]. Today, hydrogen spillover regains popularity for its importance in hydrogen storage and hydrogen fuel cells applications [13,14].

Although, the elementary mechanistic details of hydrogen spillover are not clear in most cases, it is apparent that spillover-mediated adsorption involves two fundamental processes, i.e., the dissociation of hydrogen on the metal surface and the transfer to the support. Naturally, the surface transfer of the adsorbed species is of particular interest here, although, in certain cases, diffusion through the gas phase may also be important [15,16]. Hydrogen spilt over onto the oxide support can be detected experimentally as soon as it produces OH groups or hydrogen bronzes (for example, H_xWO_3, H_xMoO_3) [11,12,17,18]. However, numerous ambiguities still exist concerning the mechanism and kinetics of the individual transfer steps. In very early work, Boudart et al. showed that in mixtures of Pt and WO_3, hydrogen spillover required the presence of molecular oxygen or water [11,12]. The mechanism and the nature of the spilt-over hydrogen were discussed controversially [1,11–13,19,20]. Hattori and Shishido [8,9] suggested that hydrogen spillover on Pt/SO_4–ZrO_2 proceeds via diffusion of neutral atoms. Those neutral atoms transform into H^+ upon donation of electrons to Lewis centers on the oxides surface. Upon reverse spillover, these electrons may be taken up again and subsequent desorption of H_2 can occur.

If spillover leads to net transfer of an atomic hydrogen species, the process is connected to a change of the oxidation state of the oxide. For reducible oxides, such as cerium dioxide, we expect a change of the oxidation state of the oxide cations [16,21,22]. As shown by Vicario et al. [21], adsorption of atomic hydrogen on CeO_2(111) is accompanied by the transfer of an electron from hydrogen to a surface cerium ion, leading to reduction of Ce^{4+} to Ce^{3+}. Spilt-over hydrogen ion situates on top of a surface oxygen ion, forming an axial tricoordinated OH group on the CeO_2(111) surface.

In the current article, we report on the direct experimental observation of hydrogen spillover using resonant photoemission spectroscopy (RPES). The method is applied to a Pt/CeO_2(111)/

* Corresponding author. Fax: +49 9131 8528867.
E-mail address: yaroslava.lykhach@chemie.uni-erlangen.de (Y. Lykhach).

0021-9517/$ - see front matter © 2011 Elsevier Inc. All rights reserved.
doi:10.1016/j.jcat.2011.09.002

Cu(1 1 1) model catalysts, and the experiment is performed under ultraclean ultrahigh-vacuum (UHV) conditions. The method allows us to monitor changes of the oxidation state of cerium with ultimate sensitivity and to determine the net charge of the spilt-over species. Thus, detailed information on the mechanism, the temperature dependence, and the reversibility of the process is obtained.

2. Experimental methods

High-resolution X-ray synchrotron radiation photoelectron spectroscopy (SRPES) studies were performed at the Materials Science Beamline at the Elettra synchrotron facility in Trieste, Italy. The ultrahigh-vacuum (UHV) end-station (base pressure 1×10^{-10} mbar) was equipped with a multichannel electron energy analyzer (Specs Phoibos 150), a rear view Low Energy Electron Diffraction (LEED) optics, an argon sputter gun, and a gas inlet system. The basic setup of the chamber includes a dual Mg/Al X-ray source used for the calibration of the energy of the synchrotron light and off-line work. Additionally, two electron-beam evaporators for metal deposition were installed on the chamber. A single crystal Cu(1 1 1) disc (MaTecK) was used as a substrate for the Pt/CeO_2 samples.

The thermal desorption spectroscopy (TDS) experiments were performed in a separate UHV system (base pressure 1×10^{-10} mbar) equipped with quadruple mass spectrometer (QMS, Pfeiffer PrismaPlus). The QMS was placed behind a differentially pumped nozzle in order to separate background contributions from molecules desorbing directly from the sample surface. The sample was heated resistively and was attached to a liquid-nitrogen cooled cryostat, making it possible to reach sample temperatures between 90 and 1200 K.

A copper single crystal, Cu(1 1 1), supplied by MaTecK GmbH (8 mm dia. disc, 2 mm thick), oriented with a miscut below 0.1° was used as the substrate. The Cu(1 1 1) was cleaned by several cycles of Ar^+ sputtering (at 300 K for 60 min) and annealing (723 K for 5 min) until no traces of carbon or any other contaminant were found in the photoelectron spectra. Epitaxial layers of CeO_2 were grown on clean Cu(1 1 1) by physical vapor deposition of Ce metal (Goodfellow, 99.99%) in an oxygen atmosphere ($p_{O_2} = 5 \times 10^{-7}$ mbar, Linde, 99.995%) at 523 K, followed by annealing of the films at 523 K in an oxygen atmosphere at the same pressure for 10 min. The preparation method yields a continuous CeO_2(1 1 1) film with a thickness of approximately 1.5 nm as determined from the attenuation of the Cu $2p_{3/2}$ intensity [23]. LEED observations on the prepared films confirm the epitaxial growth of CeO_2(1 1 1) with the characteristic (1.5×1.5) superstructure in relation to the Cu(1 1 1) substrate. According to our previous STM studies, flat CeO_2(1 1 1) terraces included extended rough patches containing small ceria particles [29]. Pt was deposited by means of physical vapor deposition from a Pt wire (0.5 mm in diameter, Goodfellow, 99.99%) onto the CeO_2/Cu(1 1 1) at 300 K. The nominal thickness of the deposited Pt layer was 0.4 nm as determined from the attenuation of the Cu $2p_{3/2}$ intensity. The structure and thermal stability of the Pt/CeO_{2-x} systems have been discussed before [29]. Briefly, Pt nanoparticles grown at 300 K preferentially nucleate at rough patches of the ceria surface. Typically, the density of Pt particles is $5.4 \pm 1.0 \times 10^{23}$ cm^{-2} and the average size of Pt particles is 3.3 ± 0.3 nm for the Pt/CeO_2 system with a nominal thickness of the Pt deposit of 0.5 nm. Valence band spectra were recorded on Pt/CeO_{2-x}/Cu(1 1 1) samples at three different photon energies, 115.0, 121.4, and 124.8 eV. Additionally, Al Kα radiation (1486.6 eV) was used to measure the core levels of O 1s, Ce 3d, and Cu $2p_{3/2}$. All spectra were acquired at constant pass energy at an emission angle for the photoelectrons of 20° and 0° with respect to the sample normal, while using the X-ray source or synchrotron radiation as appropriate. The total spectral resolutions achieved with Al Kα (1486.6 eV) and synchrotron radiation were 1 eV and 150–200 meV, respectively. The core level spectra were fitted with Voigt profile (Ce 3d, O 1s) after subtraction of a Shirley background. During the experiment, the sample temperature was controlled by a DC power supply passing a current through the Ta wires holding the sample. The actual temperature was measured by K-type thermocouple attached to the rear surface of the sample. Stable temperature and fast cooling after the annealing steps were achieved by simultaneous resistive heating and cooling of the manipulator with liquid nitrogen. The investigated samples were exposed to a total dose of hydrogen (Linde, 99.999%) of 50 L (1 L = 1.3×10^{-6} mbar × s) at 150 K. Hydrogen was dosed by backfilling the UHV chamber to a pressure of 6.6×10^{-8} mbar during 1000 s. In the first part of the experiment, the exposed samples were annealed stepwise. The annealing procedure was performed so that the sample was briefly heated to the stated temperatures and cooled down after each annealing step. In the second part, the samples were repeatedly exposed to 50 L of H_2 at constant temperatures ranging from 150 to 750 K with a step of 50 K.

The sample of Pt/CeO_2/Cu(1 1 1) used in TDS study was flash annealed to 500 K prior to hydrogen exposure in order to remove potential surface impurities (such as CO) accumulated during sample preparation.

3. Results and discussion

Essentially, RPES is based on measuring the valence band photoemission spectra at photon energies corresponding to the 4d → 4f resonance either in the Ce^{3+} or in the Ce^{4+} ions (see also [25,26] for more details). The Ce^{3+} resonance at a photon energy of 121.4 eV is caused by a Super-Coster-Kronig decay involving electron emission from Ce 4f states located about 1.4 eV below the Fermi edge. The Ce^{4+} resonance at a photon energy of 124.8 eV involves emission of O 2p electrons (hybridized with Ce states) from the valence band around 4.0 eV. Additionally, the valence band spectrum at a photon energy of 115 eV is measured corresponding to the "off-resonance" conditions. Typical valence band spectra acquired at the Ce^{3+} and Ce^{4+} resonances, as well as off-resonance, are shown in Fig. 1. The resonant enhancements for Ce^{3+} (denoted as D(Ce^{3+})) and for Ce^{4+} (D(Ce^{4+})) are quantified by calculating the intensity difference between the corresponding features in- and off-resonance. The resonant enhancement ratio (RER), calculated as D(Ce^{3+}))/(D(Ce^{4+}), is the direct measure of the change of the cerium oxidation state. Superior sensitivity of RPES in comparison with conventional XPS is illustrated in Supplementary data.

The evolution of the RER during stepwise annealing of CeO_2/Cu(1 1 1) and Pt/CeO_2/Cu(1 1 1) preexposed to 50 L of hydrogen at 150 K is displayed in Fig. 2. It was reported earlier that pristine CeO_2 does not adsorb molecular hydrogen at temperatures lower than 743 K [13]. Accordingly, no significant variation of the RER was detected for CeO_2/Cu(1 1 1). In sharp contrast, substantial and characteristic changes of the RER were observed on Pt/CeO_2/Cu(1 1 1) in the temperature region between 150 and 300 K. We designate three particular temperature regions, as indicated in Fig. 2. In the first region below 180 K, the RER remains largely unaffected. This is attributed to the fact that hydrogen dissociatively adsorbs on the Pt nanoparticles, but remains confined to the surface of the Pt particles. Spillover of hydrogen does not yet occur due to the activation barrier associated with crossing the particle boundary.

A very small initial decrease in the RER upon exposure of the sample to hydrogen at 150 K (marked with the red arrow) may be associated with attenuation of Ce^{3+} signal caused by small amounts of contaminations such as co-adsorbed water. At

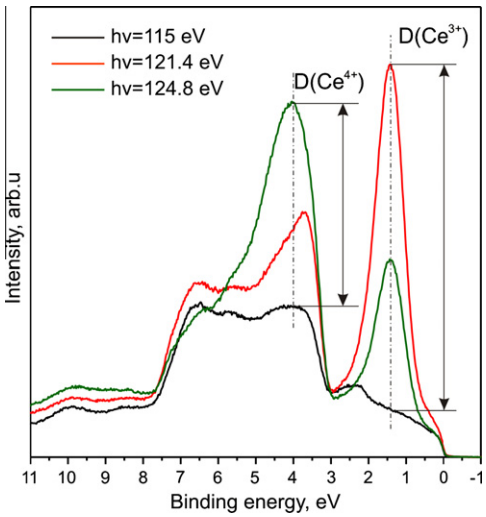

Fig. 1. Typical valence band spectra obtained on $Pt/CeO_2/Cu(1\,1\,1)$ sample containing Ce^{4+} and Ce^{3+} ions at hv = 115 eV (off-resonance mode, black line), 121.4 eV (Ce^{3+} resonance, red line), and 124.8 eV (Ce^{4+} resonance, green line). Resonant enhancement ratios (RERs), $D(Ce^{3+})$ and $D(Ce^{4+})$, are determined as intensity differences between the valence bands measured in- and off-resonance (see text). (For interpretation of the references to color in this figure legend, the reader is referred to the web version of this article.)

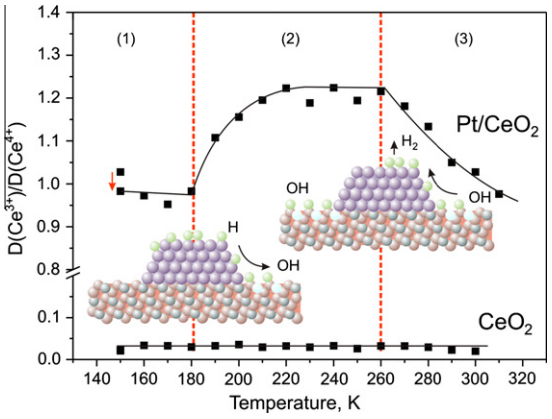

Fig. 2. Development of the RER during stepwise annealing of the $Pt/CeO_2/Cu(1\,1\,1)$ sample exposed to 50 L of hydrogen at 150 K. The inset drawings represent the situation on the surface while switching between the temperature regions. The arrow indicates the initial change of the RER upon hydrogen exposure at 150 K (see text for details).

temperatures exceeding 180 K, we observe a sharp increase in RER, followed by a plateau between 220 and 260 K. According to the mechanism discussed above, we assign these changes to the transfer of dissociated hydrogen to the support. Electron transfer from atomic hydrogen to the oxide causes reduction of Ce^{4+} to Ce^{3+} and, simultaneously, produces OH species on the CeO_2 surface [21].

Two conclusions can be derived from this observation: First, the sharp transition temperature shows that a well-defined activation barrier exists for hydrogen spillover. We tentatively attribute this barrier to the process of hydrogen crossing the particle–support boundary. Secondly, the pronounced reduction of ceria shows that the spillover involves the net transfer of neutral hydrogen species. Note that this could involve either transfer in form of neutral hydrogen via the boundary or a two step process with proton transfer via the boundary and separate electron transfer from Pt to Ce^{4+}.

In the temperature region from 260 K to 310 K, the RER decreases, finally reaching the low-temperature value again (region 3). We assign this effect to the reverse spillover of hydrogen followed by the desorption of H_2. We conclude that the hydrogen spillover and reverse spillover are processes with an activation barrier sufficiently low to be overcome even below room temperature (i.e., <260 K). A dynamic equilibrium between hydrogen on CeO_2 and hydrogen on Pt is established, leading to a constant RER as long as no hydrogen is lost (up to 260 K). As soon as the desorption temperature for hydrogen on Pt is reached, hydrogen desorbs irreversibly in the UHV experiment and is replenished by reverse spillover from the support to the Pt particles. Finally, this process leads to complete loss of hydrogen from the ceria support and, therefore, to reoxidation. Our results agree with findings of Bernal et al. who reported reversible character of reduction and recovery of the oxidation state of ceria-supported Rh catalyst at 295 K [27]. Assuming a symmetric shape of the hydrogen desorption peak, the maximum desorption would be around 285 K. This assumption is in perfect agreement with the desorption temperature of hydrogen reported for $Pt(1\,1\,1)$ [28] and observed experimentally on Pt nanoparticles supported on $CeO_2/Cu(1\,1\,1)$.

The corresponding TDS spectra of the desorption products recorded during annealing of $Pt/CeO_2/Cu(1\,1\,1)$, preexposed to 50 L of hydrogen at 150 K, are shown in Fig. 3. The dominant desorption product is molecular hydrogen. The corresponding peak develops between 150 and 450 K with a distinct maximum located at 285 K. Additionally we detected desorption of a small amount of water over a broad range of temperatures between 180 and 700 K. The observed water contains a contribution from background adsorption, which has been estimated from a blank experiment. Taking into account this correction, we estimate that the fraction of hydrogen oxidized to water does not exceed 15%.

The desorption of molecular hydrogen but not water was also observed by Cordatos et al. in similar low-temperature range (220–320 K) on Pd/CeO_2 [29].

The above finding allows us to understand the complex temperature-dependent behavior of Pt/CeO_2 in reductive atmospheres. Fig. 4 shows the results of a corresponding experiment on the $Pt/CeO_2/Cu(1\,1\,1)$ model catalyst. The experiment was performed so that the sample was repeatedly exposed to 50 L of H_2 at constant temperatures ranging from 150 to 750 K in temperature steps of 50 K.

The evolution of the RER shows a characteristic behavior (see Fig. 4). For the discussion, we differentiate between two temperature regions, designated as the regime of reversible (I, <350 K) and irreversible (II, >350 K) reduction of cerium oxide. In the low-temperature regime (I), reduction and oxidation of cerium oxide is controlled by hydrogen spillover and reverse spillover processes,

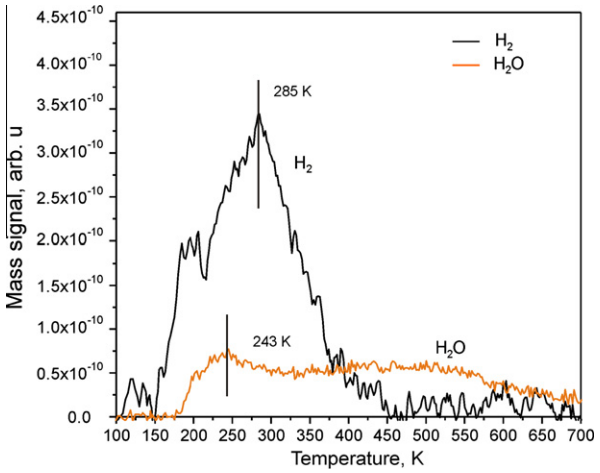

Fig. 3. TDS spectra recorded from $Pt/CeO_2/Cu(1\,1\,1)$ preexposed to 50 L of hydrogen at 150 K.

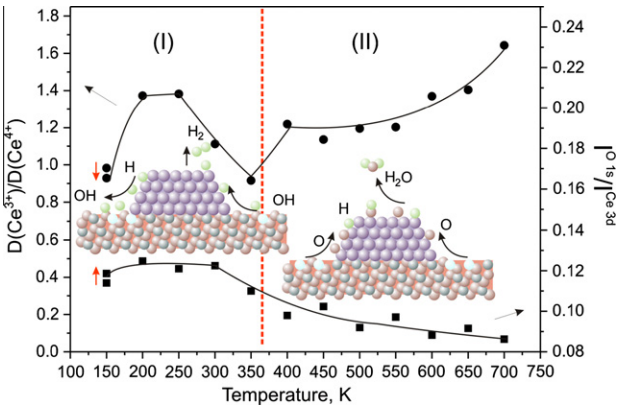

Fig. 4. Development of the RER (circles) and the ratio of the total intensity of O 1s to Ce 3d core levels (squares) upon exposure of the $Pt/CeO_2/Cu(1\,1\,1)$ model catalyst to 50 L of hydrogen at different temperatures. The inset drawings schematically depict the surface processes during reversible (I) and irreversible (II) reduction. The red arrows indicate the changes of RER and O 1s/Ce 3d intensity ratio upon hydrogen exposure at 150 K (see text for discussion). (For interpretation of the references to color in this figure legend, the reader is referred to the web version of this article.)

according to the discussion above. At 150 K, spillover is kinetically hindered and only a slight decrease in the RER is observed, mainly due to water contaminations (marked with red arrow, Fig. 4). This situation is similar to that found in region (1), Fig. 2. For H_2 exposure at 200 K, this kinetic hindrance is overcome, and hydrogen spillover leads to a substantial reduction and increase in the RER (compare region (2) in Fig. 2). In the temperature region between 300 and 350 K, the effect of H_2 on the RER is weak. According to the above discussion, this is, however, not due to the fact that hydrogen spillover does not occur. Actually, both spillover and reverse spillover are facile, but hydrogen is rapidly lost due to reverse spillover and desorption from the Pt particles.

The temperature region between 400 and 700 K corresponds to the irreversible (II) regime of ceria reduction (see Fig. 3). In accordance with our previous observations [24,30], the high-temperature region is the one where reverse spillover of oxygen is activated (above 400 K). In the presence of hydrogen, oxygen – provided by reverse spillover – reacts with hydrogen and forms water that subsequently desorbs, leading to a drastic reduction of CeO_2. The evolution of the total intensity ratio of the O 1s and Ce 3d core levels supports this scenario (see Fig. 4). The ratio remains constant below 350 K, but increases above 350 K due to reverse spillover and H_2O formation/desorption. Finally, it should be noted that at temperatures above 700 K molecular hydrogen can directly interact with cerium oxide producing water and oxygen vacancies [13,31,32].

4. Conclusions

We have demonstrated that hydrogen spillover on $Pt/CeO_2/Cu(1\,1\,1)$ involves net transfer of neutral hydrogen, either via H transfer as proposed by Hattori and Shishido [8,9] or via a multistep process. As a result, hydrogen transfer intrinsically gives rise to the formation of Ce^{3+} centers, which can be monitored with high sensitivity using RPES. Hydrogen spillover is characterized by a small but a very well-defined activation barrier, which leads to kinetic hindrance of spillover at temperatures below 180 K. The corresponding activation barrier may be associated with transport via the particle boundary. Hydrogen spillover and reverse spillover via the Pt/CeO_2 boundary becomes fully reversible at temperatures as low as 260 K. As a result, complete loss of spilt-over hydrogen and reoxidation of the ceria surface can occur due to reverse H spillover and subsequent H_2 desorption from Pt. Together with the oxygen reverse spillover, activated at above 400 K, H spillover processes provide a consistent picture of the complex changes of the oxidation state of Pt/CeO_2 surfaces in the presence of hydrogen.

Acknowledgments

The authors acknowledge financial support by the Deutsche Forschungsgemeinschaft (DFG) within the Excellence Cluster "Engineering of Advanced Materials" in the framework of the excellence initiative. We acknowledge support by the Fonds der Chemischen Industrie, the DAAD, the EU (COST D-41) and Ministry of Education of the Czech Republic (LA08022 and LC06058). Y. L and T. St. are particularly thankful to Dr. Vitaliy Feyer for technical assistance.

Appendix A. Supplementary material

Supplementary data associated with this article can be found, in the online version, at doi:10.1016/j.jcat.2011.09.002.

References

[1] W.C. Conner, J.L. Falconer, Chem. Rev. 95 (1995) 759.
[2] V.V. Rozanov, O.V. Krylov, Russ. Chem. Rev. 66 (1997) 107.
[3] G.M. Pajonk, Appl. Catal. A 202 (2000) 157.
[4] H.-W. Chen, J.M. White, J. Mol. Catal. 35 (1986) 355.
[5] P.A. Sermon, G.C. Bond, Catal. Rev. 8 (1974) 211.
[6] D. Maret, G.M. Pajonk, S.J. Teichner, Studies in Surface Science and Catalysis, Elsevier, Amsterdam, Netherlands, 1983.
[7] S.J. Khoobiar, J. Phys. Chem. 68 (1964) 411.
[8] H. Hattori, Studies in Surface Science and Catalysis, Elsevier, Kyoto, Japan, 1993.
[9] T. Shishido, H. Hattori, Appl. Catal. A 146 (1996) 157.
[10] A. Guerrero-Ruiz, I. Rodríguez-Ramos, Studies in Surface Science and Catalysis (2001).
[11] J.E. Benson, H.W. Kohn, M. Boudart, J. Catal. 5 (1966) 307.
[12] R.B. Levy, M. Boudart, J. Catal. 32 (1974) 304.
[13] G. Dutta, U.V. Waghmare, T. Baidya, M.S. Hegde, Chem. Mater. 19 (2007) 6430–6436.
[14] H. Cheng, L. Chen, A.C. Cooper, X. Sha, G.P. Pez, Energy Environ. Sci. 1 (2008) 338.
[15] F. Ahmed, M.K. Alam, R. Muira, A. Suzuki, H. Tsuboi, N. Hatakeyama, A. Endou, H. Takaba, M. Kubo, A. Miyamoto, Appl. Surf. Sci. 256 (2010) 7643.
[16] V. Amir-Ebrahimi, J.J. Rooney, J. Mol. Catal. A Chem. 159 (2000) 429.
[17] J.P. Belzunegui, J. Sanz, J.M. Guil, J. Phys. Chem. B 109 (2005) 19390.
[18] L. Chen, A.C. Cooper, G.P. Pez, H. Cheng, J. Phys. Chem. C 112 (2008) 1755.
[19] M. Boudart, J. Mol. Catal. A: Chem. 138 (1999) 319–321.
[20] U. Roland, T. Braunschweig, F. Roessner, J. Mol. Catal. A Chem. 127 (1997) 61.
[21] G. Vicario, G. Balducci, S. Fabris, S. de Gironcoli, S. Baroni, J. Phys. Chem. B 110 (2006) 19380.
[22] A. Norman, V. Perrichon, Phys. Chem. Chem. Phys. 5 (2003) 3557.
[23] F. Šutara, M. Cabala, L. Sedláček, T. Skála, M. Škoda, V. Matolín, K.C. Prince, V. Cháb, Thin Solid Films 516 (2008) 6120.
[24] Y. Lykhach, T. Staudt, M.P.A. Lorenz, R. Streber, A. Bayer, H.P. Steinrück, J. Libuda, ChemPhysChem 11 (2010) 1496.
[25] V. Matolín, I. Matolínová, L. Sedláček, K.C. Prince, T. Skála, Nanotechnology 20 (2009) 215706.
[26] V. Matolín, M. Cabala, V. Cháb, I. Matolínová, K.C. Prince, M. Škoda, F. Šutara, T. Skála, K. Veltruská, Surf. Interface Anal. 40 (2008) 225.
[27] S. Bernal, J.J. Calvino, G.A. Gifredo, J.M. Rodriguez-Izquiero, V. Perrichon, A. Laachir, J. Catal. 137 (1992) 1.
[28] N.A. Khan, L.E. Murillo, J.G. Chen, J. Phys. Chem. B 108 (2004) 15748.
[29] H. Cordatos, R.J. Gorte, J. Catal. 159 (1996) 112.
[30] G.N. Vayssilov, Y. Lykhach, A. Migani, T. Staudt, G.P. Petrova, N. Tsud, T. Skala, A. Bruix, F. Illas, K.C. Prince, V. Matolín, K.M. Neyman, J. Libuda, Nat. Mater. 10 (2011) 310.
[31] V. Perrichon, A. Laachir, G. Bergeret, F.R.L. Tournayan, J. Chem. Soc. Faraday Trans. 90 (1994) 773.
[32] H.-T. Chen, Y.M. Choi, M. Liu, M.C. Lin, ChemPhysChem 8 (2007) 849.